UCSF

Title

Modulation of myeloid and T cells in vivo by Bruton's tyrosine kinase inhibitor ibrutinib in patients with metastatic pancreatic ductal adenocarcinoma.

Permalink

https://escholarship.org/uc/item/22n0d044

Journal

ISSN

Authors

Sinha, Meenal

Betts, Courtney

Zhang, Li

et al.

Publication Date

2023

DOI

Copyright Information

![Journal for ImmunoTherapy of Cancer]

Modulation of myeloid and T cells in vivo by Bruton's tyrosine kinase inhibitor ibrutinib in patients with metastatic pancreatic ductal adenocarcinoma

Meenal Sinha [ORCID],[1] Courtney Betts,[2] Li Zhang,[1,3] Madeline J Griffith,[1] Isabelle Solman,[4] Brandon Chen,[1] Eric Liu [ORCID],[1] Whitney Tamaki,[1] Jacob Stultz,[1] Jaqueline Marquez,[1] Shamilene Sivagnanam,[2] Alexander Cheung [ORCID],[1] Denise Pener,[5] Anne Fahlman,[5] Erin Taber,[5] Kimberly Lerner,[5] Matthew Crocker,[5] Kendra Todd,[5] Brindha Rajagopalan,[5] Clarisha Ware,[1] Mark Bridge,[1] Johnson Vo,[5] Hannah Dragomanovich,[1] Julie Sudduth-Klinger,[1] Gina Vaccaro,[6] Charles D Lopez,[2,5] Margaret Tempero,[1] Lisa M Coussens,[2] Lawrence Fong[1,7]

For numbered affiliations see end of article.

Correspondence to
Dr Lawrence Fong;
lawrence.fong@ucsf.edu

ABSTRACT

Background In preclinical studies of pancreatic ductal adenocarcinoma (PDAC), ibrutinib improved the antitumor efficacy of the standard of care chemotherapy. This led to a phase 1b clinical trial to determine the safety, tolerability, and immunologic effects of ibrutinib treatment in patients with advanced PDAC.

Methods Previously untreated patients with PDAC were enrolled in a phase 1b clinical trial (ClinicalTrials.gov) to determine the safety, toxicity, and maximal tolerated dose of ibrutinib when administered with the standard regimen of gemcitabine and nab-paclitaxel. To study the immune response to ibrutinib alone, the trial included an immune response arm where patients were administered with ibrutinib daily for a week followed by ibrutinib combined with gemcitabine and nab-paclitaxel. Endoscopic ultrasonography-guided primary PDAC tumor biopsies and blood were collected before and after ibrutinib monotherapy. Changes in abundance and functional state of immune cells in the blood was evaluated by mass cytometry by time of flight and statistical scaffold analysis, while that in the local tumor microenvironment (TME) were assessed by multiplex immunohistochemistry. Changes in B-cell receptor and T-cell receptor repertoire were assessed by sequencing and analysis of clonality.

Results In the blood, ibrutinib monotherapy significantly increased the frequencies of activated inducible T cell costimulator+(ICOS+) CD4+ T cells and monocytes. Within the TME, ibrutinib monotherapy led to a trend in decreased B-cell abundance but increased interleukin-10+ B-cell frequency. Monotherapy also led to a trend in increased mature CD208+dendritic cell density, increased late effector (programmed cell death protein 1 (PD-1−) eomesodermin (EOMES+)) CD8+ T-cell frequency, with a concomitantly decreased dysfunctional (PD-1+ EOMES+) CD8+ T-cell frequency. When ibrutinib was combined with chemotherapy, most of these immune changes were not observed. Patients with partial clinical responses had more diverse T and B cell receptor repertoires prior to therapy initiation.

WHAT IS ALREADY KNOWN ON THIS TOPIC

⇒ The treatment for metastatic pancreatic cancer represents a significant unmet medical need. Treatment with ibrutinib, a Bruton's tyrosine kinase (BTK) inhibitor, was found to be beneficial in preclinical mouse models.

WHAT THIS STUDY ADDS

⇒ This clinical trial was aimed at studying whether ibrutinib could modulate immune responses in patients with metastatic pancreatic cancer. Ibrutinib monotherapy led to immunomodulatory effects in the myeloid and T cell compartments, but this effect was lost with concurrent chemotherapy.

HOW THIS STUDY MIGHT AFFECT RESEARCH, PRACTICE OR POLICY

⇒ Future studies with BTK inhibitors will need to examine improved combination strategies.

Conclusion Ibrutinib monotherapy skewed the immune landscape both in the circulation and TME towards activated T cells, monocytes and DCs. These effects were not observed when combining ibrutinib with standard of care chemotherapy. Future studies may focus on other therapeutic combinations that augment the immunomodulatory effects of ibrutinib in solid tumors.

Trial registration number NCT02562898.

INTRODUCTION

Pancreatic ductal adenocarcinoma (PDAC) represents the third leading cause of cancer-related mortality in the USA. With a 5-year relative survival rate of ~10.8%, PDAC is aggressive and difficult to treat. When first diagnosed, over 90% of patients have

advanced and inoperable disease making systemic chemotherapy the first line of treatment.

Although the combination of gemcitabine and nab-paclitaxel is a front-line standard treatment regimen for metastatic PDAC,[1] overall survival (OS) of patients is improved by only a few months. As such, further improvements in treatment are much needed. In recent years, immunotherapy for solid tumors has seen significant progress and remains an active area of immense interest for treating advanced PDAC, given the highly immuno-suppressive and tumor-promoting nature of the tumor microenvironment (TME) in this disease.[2–8] In preclinical studies using both murine pancreatic cancer cell line orthotopic graft and genetically engineered transgenic mouse models, immunomodulation via inhibition of Bruton's tyrosine kinase (BTK) with an irreversible inhibitor, ibrutinib, in combination with gemcitabine led to superior antitumor effects compared with gemcitabine alone.[9 10] In vivo, BTK expressed by both B cells and $Gr1^- CD11b^+$ myeloid cells promoted tumor growth and regulated signaling pathways that impaired $CD8^+$ T cell-dependent cytotoxicity.[9]

Based on these promising preclinical studies, a phase 1b clinical trial was conducted to evaluate the safety, efficacy, and immunomodulation of ibrutinib added to the standard regimen of gemcitabine and nab-paclitaxel for the treatment of patients with advanced PDAC. Here we report in depth the effects of ibrutinib monotherapy or combination therapy on the immune response in the blood circulation and in the TME. Some of these study findings were reported earlier as a conference abstract.[11]

METHODS
Clinical study
Patients with stage IV metastatic PDAC with no prior systemic or investigational therapy for PDAC, an intact primary tumor, Eastern Cooperative Oncology Group score of 0–1, and adequate bone marrow, hepatic, and renal functions, were enrolled into a multicenter, open-label, phase 1b study (ClinicalTrials.gov) to study the effect of one time per day, oral ibrutinib in combination with the standard regimen of gemcitabine and albumin bound paclitaxel, in the first-line therapy setting. The study consisted of a 3+3 dose escalation arm (online supplemental figure 1A) to determine the maximal tolerated dose (MTD), safety, toxicity, and antitumor effect of ibrutinib in combination with standard doses of gemcitabine and nab-paclitaxel. Grade 4 hematologic adverse events were expected with gemcitabine and nab-paclitaxel, and support with colony stimulating factor was permitted. Patients were also enrolled into an immune response arm (online supplemental figure 1B) to assess immune landscape changes in response to ibrutinib monotherapy locally in the pancreatic TME and systemically in the blood. In this arm, the patients were administered a 7-day run-in with ibrutinib alone prior to commencement of combination chemotherapy

cycles. Pre and post 7-day ibrutinib run-in treatment blood samples and endoscopic ultrasonography (EUS)-guided primary pancreatic tumor biopsies, at least 5 days before and after 7-day ibrutinib run-in, were obtained for immune response assessment. Being a challenging and invasive procedure, primary tumor biopsies could be collected only from six out of seven patients accrued. Of the collected biopsies, a post run-in biopsy was not analyzable for one of six patients. Changes in the immune landscape induced by combination treatment were studied in both study arms, but in the blood only. Progression-free survival (PFS), time-to-progression, and OS from the date of first dose of protocol therapy, were also determined. Progression was defined as radiographic and/or clinical disease progression or death. Patients were accrued at the University of California San Francisco and Oregon Health & Science University, Portland. Signed informed consent was provided by each patient. Institutional Review Boards of both institutions approved the study protocols including the collection of biospecimens.

Mass cytometry by time of flight staining and analysis
Cryopreserved peripheral blood mononuclear cells (PBMCs) isolated from blood collected from patients at various time points before and after the start of therapy were thawed, barcoded, and cytometry by time of flight (CyTOF)-stained in a single cell suspension with a panel of ~40 different heavy metal-tagged antibodies that were either purchased (Fluidigm) or conjugated with heavy metal in-house (see online supplemental tables 1–3 for CyTOF reagents and staining panels). The stained cells were washed and run through a Helios instrument (Fluidigm) to acquire data. The data collected was pre-processed for bead-based signal normalization and subsequently debarcoded using the Premessa R package (https://github.com/ParkerICI/premessa). PBMCs that were singlets, live (intercalator$^+$ cisplatin$^-$), $CD45^+$, and red blood cell (RBC$^-$) and platelet-free ($CD61^-$ $CD235ab^-$) (online supplemental figure 2) were extracted as new Flow Cytometry Standard (FCS) files in Cytobank (Beckman Coulter), and analyzed by unsupervised clustering into 200 clusters using the statistical scaffold R package (https://github.com/SpitzerLab/statisticalScaffold) for significant changes in the immune landscape in response to treatment or based on patient clinical responses.[12 13] Clusters were arranged around landmark nodes, which are cell types manually gated (see online supplemental figure 2 for manual gating strategy) and extracted as individual fcs files, based on similarity in force-directed scaffold maps. Cluster frequencies and boolean expression for functional markers for each cluster were passed through the Significance Across Microarrays (samr) algorithm and results were formulated into the scaffold maps for visualization. For scaffold heatmaps, fold change, significance, cell count, and nearest landmark node data were extracted from the scaffold analysis outputs using a custom script. The heat map was created in R using pheatmap (https://CRAN.

R-project.org/package=pheatmap), with $\log_2$ fold change capped at −2 to 2.

Annotated Uniform Manifold Approximation and Projection (UMAP) plots were created using Cytobank's dimensionality reduction suite. Starting with preprocessed fcs files for singlet, live, RBC– and platelet-free $CD45^+$ cells as input, 80,000 cells were randomly sampled from each of the 15 fcs files used as input (corresponding to 15 samples from six patients over three time points) for a total of 1.2 million cells. The channels for CCR7, CD117, CD11b, CD11c, CD123, CD127, CD14, CD15, CD16, CD19, CD25, CD3, CD31, CD33, CD38, CD4, CD45RA, CD56, CD61, CD235ab, CD8a, FcεR1α, FOXP3, HLA-DR, podoplanin, TCR-Va24-Ja18, TCRγδ, and VISTA were selected as input for the UMAP dimensionality reduction algorithm. For the UMAP algorithm parameters, the defaults were retained: number of neighbors=15, minimum distance=0.01, and collapse outliers=yes. Finally, prior to dimensionality reduction, the values in each channel were normalized to a mean of 0 and SD of 1. Nine cell populations were manually gated on the UMAP plot with cell-specific expression markers. Traditional gating in Cytobank was also used to identify and analyze various cell populations and their functional states.

For some of the patient blood draws, absolute monocyte counts were collected as part of the complete blood count (CBC) analysis.

Multiplex immunohistochemistry

EUS-guided primary tumor biopsies obtained before and after ibrutinib monotherapy were sectioned and stained using multiplex immunohistochemistry (mIHC). Twenty different immune cell types and their functional states were identified using a computational pipeline concluding with hierarchical gating via image cytometry.

Sequential immunohistochemistry was performed on 5 μm formalin-fixed paraffin-embedded (FFPE) sections using three antibody panels as previously described.[14 15] Briefly, slides were processed by deparaffinization, heat-mediated antigen retrieval in pH 6.0 Citra solution (BioGenex, Fremont, California, USA), blocking in Dako Dual Endogenous Enzyme Block (S2003, Dako, Santa Clara, California, USA), and protein blocking with 5% normal goat serum and 2.5% bovine serum albumin (BSA) in tris-buffered saline-0.1% Tween (TBST). Primary antibodies were applied in sequential order as described previously[16] with the addition of CSF1R (Abcam, cat. no. ab183316; 1:150 dilution for 30 min at room temperature at cycle 0, round 1, prior to antigen retrieval) to the myeloid panel and interleukin (IL)-10 (LifeSpan BioSciences, cat. no. 501505; 1:25 dilution, 4°C overnight, cycle 6, round 3) to the functional B-cell panel. After washing off primary antibody in TBST, either anti-rat, anti-mouse, or anti-rabbit Histofine Simple Stain MAX PO horseradish peroxidase-conjugated polymer (Nichirei Biosciences, Tokyo, Japan) was applied for 30 min at room temperature, followed by AEC chromogen (Vector Laboratories, Burlingame, California, USA). Whole slide digital imaging was performed following each chromogen development. Heat and chemical stripping between cycles and rounds was performed as previously described. DNA was stained with hematoxylin (S330130-2, Dako, Santa Clara, California, USA) for the purposes of image computation.

Regions of interest were selected, and then images were co-registered in MATLAB V.R2018b using the SURF algorithm in the Computer Vision Toolbox (The MathWorks, Natick, Massachusetts, USA). Image processing and cell quantification were performed using FIJI (FIJI Is Just ImageJ)[17] and CellProfiler V.3.5.1.[18] AEC signal was extracted for quantification and visualization in FIJI using a custom macro for color deconvolution. Briefly, the FIJI plugin Color_Deconvolution (H AEC) was used to separate hematoxylin, followed by post-processing steps for signal cleaning and background elimination. AEC signal was extracted in FIJI using the NIH plugin RGB_to_CMYK. Color deconvoluted images were processed in CellProfiler to quantify single cell mean intensity signal measurements for every stained marker. CellProfiler outputs were loaded into FCS Express 7 Image Cytometry RUO (De Novo Software, Glendale, California, USA) software, and hierarchical gating was performed as previously[16] to classify immune cell populations, with the addition of CSF1R and IL-10 as terminal gates in the myeloid and lymphoid panels, respectively.

BCR and TCR sequencing

T-cell receptor (TCR) β chains and immunoglobulin heavy chain CDR3 regions were amplified and sequenced using 2 μg of genomic DNA (or all available extracted DNA if the amount was <2 μg) by Adaptive Biotechnologies using the immunoSEQ platform. B-cell receptor (BCR) and TCR data analysis was performed using the TCR3D software developed.[19] Only clones with ≥5 count were analyzed. Diversity of the BCR and TCR repertoire at each time point was measured by clonality on a scale of 0–1, where 0 indicates total diversity (ie, all BCR/TCR clonotypes equally common) and 1 indicates no diversity (ie, the BCR/TCR repertoire is dominated by a single clone). Clonality can be considered as a normalized Shannon entropy index (H) over the number of unique clones (n): Clonality=1 − $H/\log_e(n)$, where $H/\log_e(n)$ is Pielou's evenness (equability).[20] The proportion of newly generated clones was calculated as the ratio of the number of newly generated clones versus the total number of clones at C2D1 of combination therapy versus screen. Per cent change in BCR and TCR clonality with ibrutinib monotherapy was calculated as a ratio of the clonality after treatment (post) to that before treatment (pre) time points. Data was presented as box plots with median and IQR. Two group comparisons were performed using Wilcoxon rank-sum test for continuous matrices, while the comparison between two different time points were done by Wilcoxon signed-rank test. OS was estimated by the Kaplan-Meier method. The relationship between OS and BCR and TCR features was analyzed using a log-rank test. P value<0.05 was statistically significant; no multiple testing adjustment was done. The BCR and TCR

analysis was done with the software R V.4.0.5 (https://www.r-project.org/).

BTK occupancy assay

Lysates from cryopreserved patient PBMCs collected at various time points before and after therapy were assessed by Pharmacyclics (an AbbVie company) for ibrutinib-induced BTK inhibition or occupancy using an ELISA-based assay as described earlier.[21] Free and total BTK were measured, which was used to determine the percentage of ibrutinib-inactivated BTK. Per cent BTK occupancy was defined as 100 − (free BTK×100/total BTK) and was normalized to that at the screen time point for each patient.

Statistical considerations and analysis

Data from traditional cellular gating and mIHC were plotted as mean±SEM in bar graphs using GraphPad Prism V.9 and tested for statistical significance by Wilcoxon matched-pairs signed rank test. When matched-pair CyTOF and mIHC data was segregated by low and high BTK occupancy, Friedman test was used. Mann-Whitney test was used to determine statistically significant association between cell features in PBMCs and clinical response. All p values are two-sided, and $p < 0.05$ was accepted as statistically significant.

RESULTS
Study design

In this phase 1b, open-label study, patients with previously untreated metastatic PDAC were administered the combination regimen of ibrutinib, gemcitabine, and nab-paclitaxel in the dose escalation arm (online supplemental figure 1A). In the immune response arm (online supplemental figure 1B), patients were first given a once-daily ibrutinib alone run-in for 7 days, which was followed by ibrutinib in combination with the standard treatment regimen of gemcitabine and nab-paclitaxel. The safety, toxicity, and MTD of ibrutinib when administered in combination with the standard regimen was determined in the dose escalation arm using a 3+3 dosing design. In the immune response arm, the effect of 7-day treatment with ibrutinib alone on leukocytes in the peripheral blood and in the PDAC TME was evaluated. The MTD for ibrutinib was determined to be 560 mg/day (data not shown). The frequency of leukocytes in the blood (online supplemental figure 3A) and in the TME (online supplemental figure 3C) pre and post 7-day ibrutinib only treatment is summarized for each patient as stacked bar graphs.

Patient baseline characteristics, safety, and efficacy

Ten patients consented to and were treated in the dose escalation cohort (table 1). Of the 14 patients that consented to the immune response arm, 3 failed the screen, 8 were treated and 2 withdrew, 1 of whom withdrew post-first biopsy but before the ibrutinib run-in while the other 1 withdrew mid-ibrutinib monotherapy.

Table 1 Baseline patient demographics

Baseline characteristics	Dose escalation cohort (n=10)	Immune response cohort (n=7)
Age (years), median (range)	58 (45–80)	69 (53–81)
Sex, n (%)		
Male	4 (40)	4 (57)
Female	6 (60)	3 (43)
Race, n (%)		
White	6 (60)	6 (85.7)
Native American or Alaska Native	0 (0)	1 (14.3)
Native Hawaiian or Pacific Islander	1 (10)	0 (0)
Asian	1 (10)	0 (0)
Unknown	2 (20)	0 (0)
Ethnicity, n (%)		
Non-Hispanic	8 (80)	7 (100)
Hispanic or Latino	2 (20)	0 (0)
ECOG PS, n (%)		
0	6 (60)	2 (28.6)
1	4 (40)	5 (71.4)
Study site, n (%)		
UCSF	9 (90)	1 (12.5)
OHSU	1 (10)	6 (87.5)
Smoking, n (%)		
Current smoker	0 (0)	2 (28.6)
Ex-smoker	4 (40)	2 (28.6)
Non-smoker	6 (60)	3 (42.8)
Alcohol use, n (%)		
Yes	3 (30)	1 (12.5)
No	7 (70)	6 (87.5)

ECOG PS, Eastern Cooperative Oncology Group performance score; OHSU, Oregon Health & Science University; UCSF, University of California San Francisco .

The patients across the two arms had very similar baseline characteristics (table 1). None of the patients had a genetic predisposition syndrome nor a family history of PDAC (data not shown in the table). All patients in the study were confirmed to have adequate bone marrow, hepatic and renal functions. Patients in the immune response arm had an intact primary tumor.

The combination treatment was generally well tolerated, and serious adverse events (online supplemental table 5) and other adverse events (online supplemental table 6) in study patients were expected with gemcitabine and nab-paclitaxel, ibrutinib, or could be attributable to the underlying disease occurred in study patients. Of 14 study patients with available clinical response information, 3 had a partial clinical response, 2 had progressive

disease, and 9 had stable disease. Time to progression, OS and PFS have been summarized in online supplemental table 6.

Ibrutinib impacted B-cell abundance and function

A representative UMAP resulting from dimensionality reduction of CyTOF-stained patient PBMCs is shown (figure 1A, left panel). Cell types identified by cell type-specific markers are color-coded. Frequencies of each cell type pre-ibrutinib and post-ibrutinib monotherapy are summarized as stacked bar graphs per patient (figure 1A, right panel).

In the immune response arm (online supplemental figure 1B), ibrutinib monotherapy reduced B-cell frequency in the blood on average when compared with the frequency pretherapy (figure 1B, left panel), although this did not reach statistical significance. When examining patient-specific responses, only two of five patients had reduced B cells percentages (figure 1B, right panel). Since BTK occupancy, a measure of target inhibition achieved by ibrutinib treatment, was evaluated for at least a subset of the patients (online supplemental figure 4), correlation of BTK occupancy with changes in leukocyte frequencies was assessed. In the immune response arm, two patients had a 'low' BTK occupancy (42% and 62%) while two patients had a 'high' BTK occupancy (84% and 85%) at the post-ibrutinib time point (online supplemental figure 4A). Ibrutinib-induced B-cell frequency changes did not correlate with BTK occupancy (figure 1C, left and right panels). Further, scaffold analysis did not reveal significant functional changes in B cells, except a significant increase in Ki-67+ cells in a small B-cell cluster after ibrutinib monotherapy (figure 1D).

In the TME, B cells often co-located with $CD8^+$ T cells (figure 1E). B-cell abundance trended towards reduction after ibrutinib monotherapy (figure 1F, left panel), with clear reductions in three out of five patients (figure 1F, right panel). When enumerating the percentages of B cells of total $CD45^+$ cells in the TME, patients with high BTK occupancy exhibited greater reductions in B cell frequencies (figure 1G, left and right panels). Only one patient (figure 1, data points in beige/tan) exhibited B-cell frequency reductions in both the circulation and tumor tissue. Interestingly however, all evaluable patients exhibited increased prevalence of $IL-10^+$ B cells, potentially B regulatory cells (B_{regs}), in the TME (figure 1H, left and right panels). A representative image of tissue-stained $IL-10^+$ B cells is shown in online supplemental figure 5A.

Myeloid cell abundance and function were elevated by ibrutinib peripherally and locally

All populations of circulating monocytes, that is, classical, intermediate, and non-classical, trended towards an increase in frequency after ibrutinib monotherapy (figure 2A). When segregating patients by BTK occupancy post-ibrutinib, monocyte populations increased to a greater extent in the high BTK occupancy rather than the low BTK occupancy group (figure 2B). In

addition, scaffold analysis revealed statistically significant frequency increases in seven different monocyte clusters in PBMCs after ibrutinib monotherapy (figure 2C). Further, absolute monocyte counts in blood, collected as part of CBC counts for only one of the patients, increased after ibrutinib (pre=0.86×10^9/L, post=1.72×10^9/L). Similarly, conventional dendritic cells (cDCs) trended towards increased frequency post-ibrutinib (figure 2D, left panel). In addition, patients with high BTK occupancy displayed greater increases in cDC frequency when compared with the low BTK occupancy patients (figure 2D, right panel). In contrast, there were no changes or trends in frequencies of cDC1, $Fc\varepsilon R1\alpha^+$ cDC or plasmacytoid DCs (online supplemental figure 5B,C) after Ibrutinib monotherapy. Scaffold analysis did not reveal any functional changes such as activation or maturation in the monocyte or dendritic cell (DC populations in the periphery however (data not shown).

In the tumor tissue, although there was no change in the overall abundance of total DCs (figure 2E, left panel), there was a trend towards increased abundance in patients with high versus low BTK occupancy (figure 2E, right panel). Interestingly, DCs in the PDAC TME tended to reflect a more mature phenotype, as measured by positive expression of DC-LAMP (CD207), after ibrutinib monotherapy (figure 2F; online supplemental figure 5E) with no correlation of DC maturation with BTK occupancy (online supplemental figure 5D, left and right panels).

Ibrutinib reduced T-cell abundance but increased T-cell activation

Ibrutinib monotherapy led to an overall trend of reduced frequencies of all $CD3^+$ T cells, including subsets such as $CD4^+$ T cells, $CD8^+$ T cells, and regulatory T cells (Tregs) in blood (online supplemental figure 6A). Reduction in the T cell types was more pronounced with 'high' BTK occupancy (online supplemental figure 6B). Similar observations were made when analyzing naïve, effector, central memory and effector memory subpopulations of both $CD4^+$ T (online supplemental figure 6C,D) and $CD8^+$ T cells (online supplemental figure 6E,F) for the whole cohort of patients, and when grouping by BTK occupancy.

Scaffold analysis of functional marker expression on peripheral blood T cells was performed to assess any functional changes in T cells that were induced by ibrutinib monotherapy. This revealed significantly increased frequencies of $CD4^+$ T but not $CD8^+$ T cells positive for inducible T cell costimmulator (ICOS), a T-cell activation marker (figure 3A,B). Among $CD4^+$ T cells, the significant increase in ICOS-positive cell frequency was observed across several clusters of $CD4^+$ central memory, $CD4^+$ effector, $CD4^+$ effector memory and Tregs, but not $CD4^+$ naïve T cells (figure 3A,B). Ibrutinib also significantly increased the frequency of $Ki-67^+$ cells in a $CD8^+$ effector memory cluster (figure 3A). The findings from scaffold were confirmed by traditional cytometry gating for ICOS on T cells pre-ibrutinib (figure 3C, upper panel) and post-ibrutinib (figure 3C, lower panel). As expected, various $CD4^+$ T cell types (figure 3D, F and G–J),
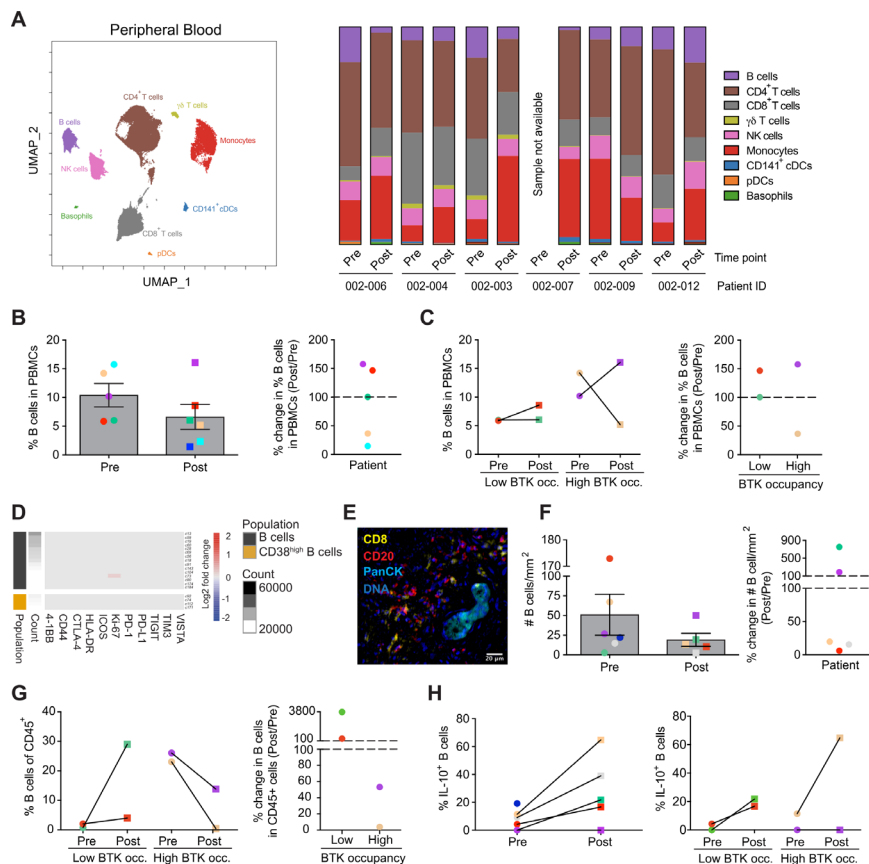
Figure 1 Changes in B-cell abundance and function with ibrutinib treatment. (A) Left panel, A representative Uniform Manifold Approximation and Projection (UMAP) plot of a patient PBMC sample from the immune response arm of the study (see online supplemental figure 1B for study schema) is shown. Clusters corresponding to various cell types identified (B cells, CD4+ T cells, CD8+ T cells, γδ T cells, NK cells, monocytes, CD141+ conventional dendritic cells (cDCs), plasmacytoid dendritic cells (pDCs) and basophils) are represented using distinct colors on the UMAPs. Right panel, the percentages of the cell types identified in the UMAP in the left panel are shown as stacked bars, totaling to 100%, for each patient sample, pre-ibrutinib and post-ibrutinib, in the immune response arm of the study. B cell changes in the peripheral blood (B–D) and tumor tissue (E–H) from patients treated daily with ibrutinib for 1 week in the immune response arm are shown. Each colored symbol (pre-ibrutinib=round; post-ibrutinib=square) consistently represents a unique patient in the study. (B) Left panel, bar graphs for B-cell frequency in blood pre-ibrutinib and post-ibrutinib monotherapy (n=5 pre-ibrutinib and 6 post-ibrutinib patient samples). Right panel, per cent change in B-cell frequency per patient (post/pre); increases are above the line at the 100-mark, while decreases are below (n=5 patients). (C) Left panel, paired samples for B-cell frequency in blood pre-ibrutinib and post-ibrutinib, grouped by low and high BTK occupancy (n=4 patients). Right panel, per cent change in B-cell frequency (post/pre) grouped by low and high BTK occupancy; increases are above the line at the 100-mark, while decreases are below (n=4 patients). (D) Scaffold analysis heatmap of $\log_2$ fold changes, post-ibrutinib monotherapy, in the frequency of B cells positive for functional markers 4-1BB, CD44, CTLA-4, HLA-DR, ICOS, Ki-67, PD-1, PD-L1, TIGIT, TIM3, and VISTA (n=5 pre-ibrutinib and 6 post-ibrutinib patient samples). Each row represents a unique B-cell cluster or a CD38high B-cell cluster. The clusters are ordered by abundance within each cell type. Each column represents a functional marker wherein the color-coding represents clusters that showed a significant $\log_2$ fold change (q<0.05) in the frequency of cells positive for that functional marker, with red being significantly higher while blue being significantly lower post-treatment. The intensity of the color code is proportional to the $\log_2$ fold change and is capped at a range of 2 and –2. Gray cells represent clusters with no statistically significant changes. (E) Representative pseudo-colored mIHC image of tumor tissue showing CD20+ B cells (red) and CD8+ T cells (yellow) close to tumor cells (light blue). (F) Left panel, bar graphs of B-cell density (number of B cells per mm^2 of tumor tissue area) in biopsies pre-ibrutinib and post-ibrutinib monotherapy (n=6 pre-ibrutinib and 5 post-ibrutinib patient samples). Right panel, per cent change in B-cell density per patient (post/pre); increases are above the line at the 100-mark, while decreases are below (n=5 patients). (G) Left panel, percentage of B cells in CD45+ cells in tumor biopsies pre-ibrutinib and post-ibrutinib monotherapy, grouped by low and high BTK occupancy (n=4 patients). Right panel, per cent change in B-cell frequency in CD45+ cells per patient (post/pre) grouped by low and high BTK occupancy. Increases are above the line at the 100-mark, while decreases are below (n=4 patients). (H) Left panel, paired samples for IL-10+ CD20+ B-cell frequency in tumor pre-ibrutinib and post-ibrutinib (n=6 pre-ibrutinib and 5 post-ibrutinib patient samples). Right panel, paired samples for IL-10+ CD20+ B-cell frequency in tumor pre-ibrutinib and post-ibrutinib, grouped by low and high BTK occupancy (n=4 patients). Data plotted on bar graphs are mean±SEM; statistical significance was tested by Wilcoxon matched-pairs signed-rank test. Friedman test was used to test for statistical significance of matched-pair data segregated by BTK occupancy. *p<0.05; **p<0.01; ***p<0.005. BTK, Bruton's tyrosine kinase; IL, interleukin; NK, natural killer; PBMCs, peripheral blood mononuclear cells.
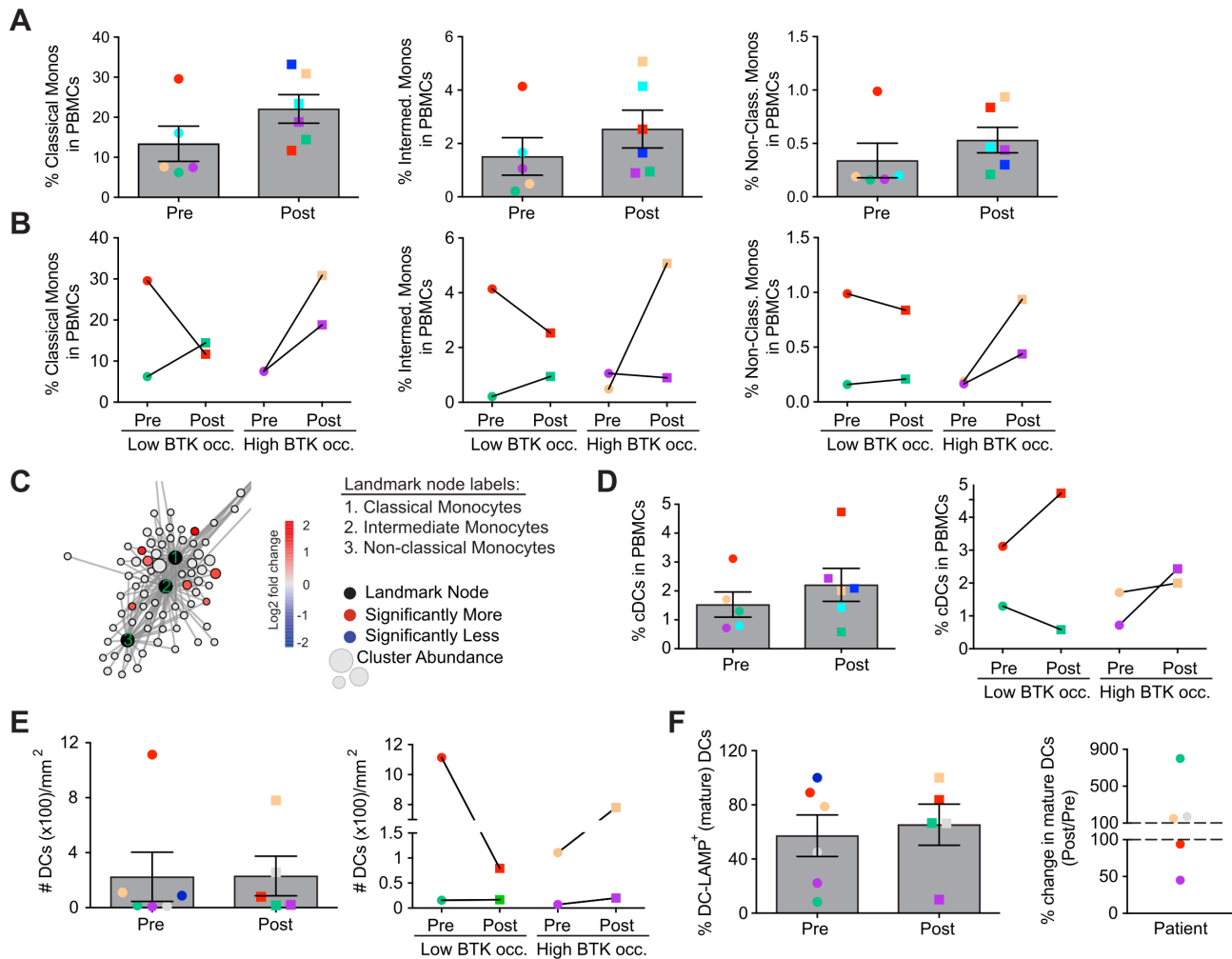
Figure 2 Impact of ibrutinib treatment on myeloid cell abundance and function. Shown are changes in myeloid cells in the peripheral blood (A–D) and tumor tissue (E–F) from patients treated with ibrutinib for 1 week in the immune response arm (see online supplemental figure 1B for study schema). Each colored symbol (pre-ibrutinib=round; post-ibrutinib=square) consistently represents a unique patient in the study. (A) Left panel, bar graphs of classical monocyte frequency in blood pre-ibrutinib and post-ibrutinib monotherapy. Middle panel, bar graphs of intermediate monocyte frequency in blood pre-ibrutinib and post-ibrutinib monotherapy. Right panel, bar graphs of non-classical monocyte frequency in blood pre-ibrutinib and post-ibrutinib monotherapy (n=5 pre-ibrutinib and 6 post-ibrutinib patient samples). (B) Left panel, paired samples for classical monocyte frequency in blood pre-ibrutinib and post-ibrutinib, grouped by low and high BTK occupancy. Middle panel, paired samples for intermediate monocyte frequency in blood pre-ibrutinib and post-ibrutinib, grouped by low and high BTK occupancy. Right panel, paired samples for non-classical monocyte frequency in blood pre-ibrutinib and post-ibrutinib, grouped by low and high BTK occupancy (n=4 patients). (C) Zoomed-in scaffold map view of monocyte clusters in the blood (see online supplemental figure 3B for complete scaffold map) showing significantly increased abundance of monocyte clusters (red colored; q<0.05) after ibrutinib monotherapy. Black circles on the scaffold map represent landmark nodes that are cell types identified by traditional manual gating. The surrounding circles represent cell clusters identified in patient samples by unsupervised clustering by the machine learning algorithm of scaffold. The size of the circle is proportional to cellular abundance. The lines represent the connections of clusters to landmark nodes based on phenotypic similarity with the length being proportional to the phenotypic similarity (n=5 pre-ibrutinib and 6 post-ibrutinib patient samples). (D) Left panel, bar graphs of conventional dendritic cell (cDC) frequency in PBMCs pre-ibrutinib and post-ibrutinib treatment (n=5 pre-ibrutinib and 6 post-ibrutinib patient samples). Right panel, paired samples for cDC frequency in blood pre-ibrutinib and post-ibrutinib, grouped by low and high BTK occupancy (n=4 patients). (E) Left panel, bar graphs for dendritic cell (DC) density (number of DCs per mm^2 of tumor tissue area) in tumor biopsies pre-ibrutinib and post-ibrutinib monotherapy (n=6 pre-ibrutinib and 5 post-ibrutinib patient samples). Right panel, paired patient data for DC density in tumor tissue pre-ibrutinib and post-ibrutinib, grouped by low and high BTK occupancy (n=4 patients). (F) Left panel, bar graphs of frequency of DCs that were DC-LAMP+, a DC maturity marker, in biopsies pre-ibrutinib and post-ibrutinib monotherapy (n=6 pre-ibrutinib and 5 post-ibrutinib patient samples). Right panel, per cent change in frequency of DC-LAMP+ DCs per patient (post/pre); data points above the 100-mark line signify increases, while those below signify decreases after ibrutinib (n=5 patients). Data plotted on bar graphs are mean±SEM; statistical significance was tested by Wilcoxon matched-pairs signed-rank test. Friedman test was used to test for statistical significance of matched-pair data segregated by BTK occupancy. *p<0.05; **p<0.01; ***p<0.005. BTK, Bruton's tyrosine kinase; LAMP, lysosome-associated membrane glycoprotein; PBMCs, peripheral blood mononuclear cells.
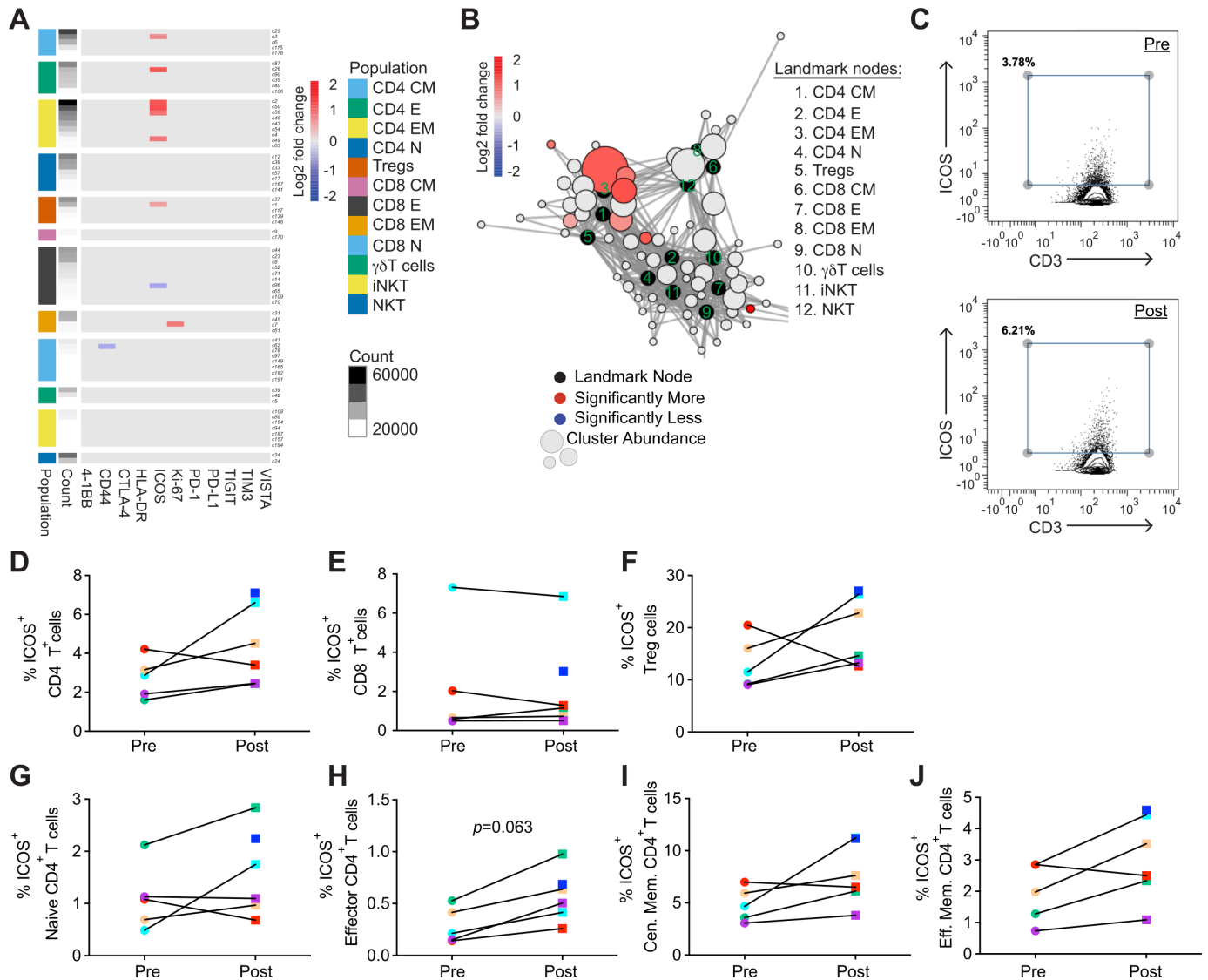
Figure 3 Changes induced by ibrutinib treatment in T-cell abundance and function in blood. Shown are changes in T cells in the PBMCs of patients treated with ibrutinib for a week in the immune response arm (see online supplemental figure 1B for study schema). Each colored symbol (pre-ibrutinib=round; post-ibrutinib=square) consistently represents a unique patient in the study. (A) Scaffold analysis heatmap of $\log_2$ fold changes, post-ibrutinib monotherapy, in the frequency of T cell clusters positive for functional markers 4-1BB, CD44, CTLA-4, HLA-DR, ICOS, Ki-67, PD-1, PD-L1, TIGIT, TIM3, and VISTA (n=5 pre-ibrutinib and 6 post-ibrutinib patient samples). Each row represents a unique T-cell cluster with the closest landmark node to that cluster designated by the color codes in the population legend (CM, central memory; E, effector; EM, effector memory; N, naïve). The clusters are ordered by abundance, high to low, within each landmark node type. Each column represents a functional marker wherein the color-coding represents clusters that showed a significant $\log_2$ fold change (q<0.05) in the frequency of cells positive for that functional marker, with red being significantly higher while blue being significantly lower post-treatment. The intensity of the color code is proportional to the $\log_2$ fold change and is capped at a range of 2 and –2. Gray cells represent clusters with no statistically significant changes. (B) Zoomed-in scaffold map view of T cell clusters (see online supplemental figure 3B for complete scaffold map) (n=5 pre-ibrutinib and 6 post-ibrutinib patient samples). Black circles on the scaffold map represent landmark nodes that are cell types identified by traditional manual gating. The surrounding circles represent cell clusters identified in patient samples by unsupervised clustering by the machine learning algorithm of scaffold. The size of the circle is proportional to cellular abundance. The lines represent the connections of clusters to landmark nodes based on phenotypic similarity with the length being proportional to phenotypic similarity. Shown in red are the clusters that had significantly increased frequency of ICOS-positive T cells after ibrutinib monotherapy. The color-coding represents clusters that exhibited significant differences (q<0.05; red=increase, blue=decrease) in parameters assessed (cellular frequency or frequency of functional marker-positive cells) between two different groups. (C) Representative dot plots showing ICOS-positive T cells in PBMCs pre (top panel) and post (bottom panel) 1 week ibrutinib treatment. Paired pre-ibrutinib and post-ibrutinib PBMC sample plots for frequency of ICOS-positive CD4^{+} T cells (D), CD8^{+} T cells (E), Tregs (F), naïve CD4^{+} T cells (G), effector CD4^{+} T cells (H), central memory CD4^{+} T cells (I) and effector memory CD4^{+} T cells (J) (n=5 pre-ibrutinib and six post-ibrutinib patient samples for panels (D–J). Statistical significance was tested by Wilcoxon matched-pairs signed-rank test. *p<0.05; **p<0.01; ***p<0.005. ICOS, inducible T cell costimulator; PBMC, peripheral blood mononuclear cell; Tregs; regulatory T cells.
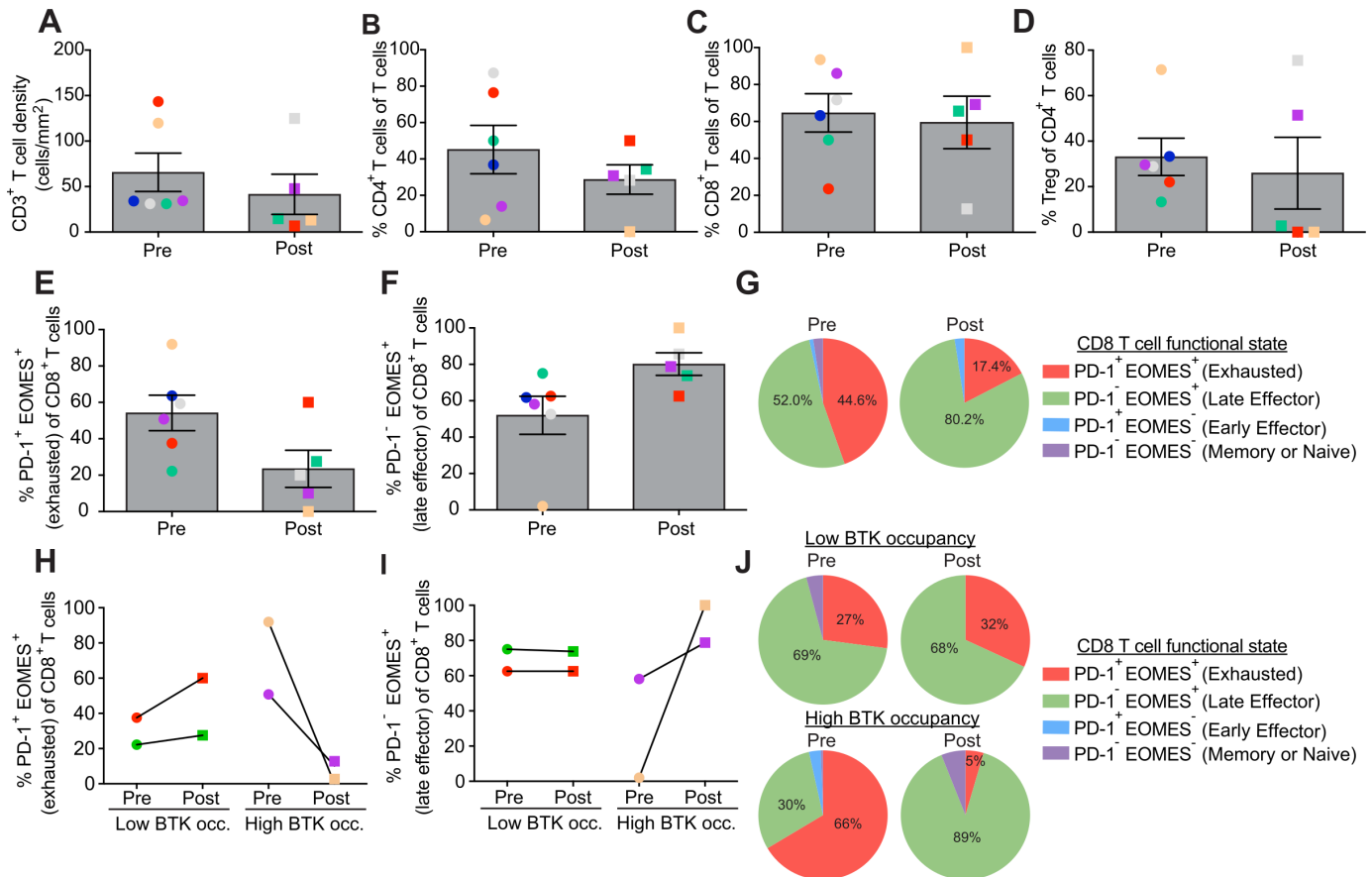
Figure 4 Changes induced by ibrutinib treatment in T-cell abundance and function in the tumor. Shown are changes in T cells in the tumor tissue of patients treated with ibrutinib for 1 week in the immune response arm (see online supplemental figure 1B for study schema). Each colored symbol (pre-ibrutinib=round; post-ibrutinib=square) consistently represents a unique patient in the study. Bar graphs of (A) total T-cell density (number of CD3$^+$ T cells per mm^2 of tumor tissue area), (B) per cent CD4$^+$ T cells of total T cells, (C) per cent CD8$^+$ T cells of total T cells, and (D) per cent Treg cells of total T cells in tumor tissue pre-ibrutinib and post-ibrutinib treatment. (E) Bar graphs of per cent CD8$^+$ T cells with PD-1$^+$ EOMES$^+$ exhausted phenotype in tumor tissue pre-ibrutinib and post-ibrutinib treatment. (F) Bar graphs of per cent CD8$^+$ T cells with PD-1$^-$ EOMES$^+$ late effector phenotype in tumor tissue pre-ibrutinib and post-ibrutinib treatment. (G) Pie charts showing average frequencies of CD8$^+$ T cells that are exhausted (PD-1$^+$ EOMES$^+$), late effector (PD-1$^-$ EOMES$^+$), early effector (PD-1$^+$ EOMES$^-$) and memory or naïve (PD-1$^-$ EOMES$^-$) in patients' tumor tissues pre-ibrutinib and post-ibrutinib treatment (panels A–G: n=6 pre-ibrutinib and 5 post-ibrutinib patient samples). Paired samples for (H) per cent CD8$^+$ T cells with PD-1$^+$ EOMES$^+$ exhausted phenotype, and (I) per cent CD8$^+$ T cells with PD-1$^-$ EOMES$^+$ late effector phenotype in tumor tissue pre-ibrutinib and post-ibrutinib, grouped by low and high BTK occupancy. (J) Pie charts showing average frequencies of CD8$^+$ T cells that are exhausted (PD-1$^+$ EOMES$^+$), late effector (PD-1$^-$ EOMES$^+$), early effector (PD-1$^+$ EOMES$^-$) and memory or naïve (PD-1$^-$ EOMES$^-$) in patients' tumor tissues pre-ibrutinib and post-ibrutinib treatment, grouped by low and high BTK occupancy (panels H–J: n=4 patients). Data plotted on bar graphs are mean±SEM; statistical significance was tested by Wilcoxon matched-pairs signed-rank test. Friedman test was used to test for statistical significance of matched-pair data segregated by BTK occupancy. *p<0.05; **p<0.01; ***p<0.005. BTK, Bruton's tyrosine kinase; EOMES, eomesodermin; PD-1, programmed cell death protein-1, Tregs, regulatory T cells.

but not CD8$^+$ T cells (figure 3E, online supplemental figure 6G) trended towards increased frequency of ICOS$^+$ cells. No significant changes were observed in the majority of the other functional markers studied (figure 3A).

As was observed in the peripheral blood, frequencies of all T cells (figure 4A), CD4$^+$ T cells (figure 4B), CD8$^+$ T cells (figure 4C) and Tregs (figure 4D) trended towards a reduction in the TME. However, no clear correlation was observed between T-cell frequency changes and BTK occupancy (data not shown). Functionally, ibrutinib trended to reduce the frequency of dysfunctional (programmed cell death protein 1 (PD-1$^+$) eomesodermin (EOMES$^+$))

CD8$^+$ T cells (figure 4E,G, red pie) and increased the frequency of late effector (PD-1$^-$) EOMES$^+$) CD8$^+$ T cells (figure 4F,G, green pie) in the TME. Further, the reduction in dysfunctional (figure 4H,J, red pie) and increase in late effector CD8$^+$ T cells (figure 4I,J, green pie) was greater in patients with high BTK occupancy.

Combination therapy with ibrutinib, gemcitabine and nab-paclitaxel led to increased frequency of monocytes and reduced frequency of natural killer cells in the blood

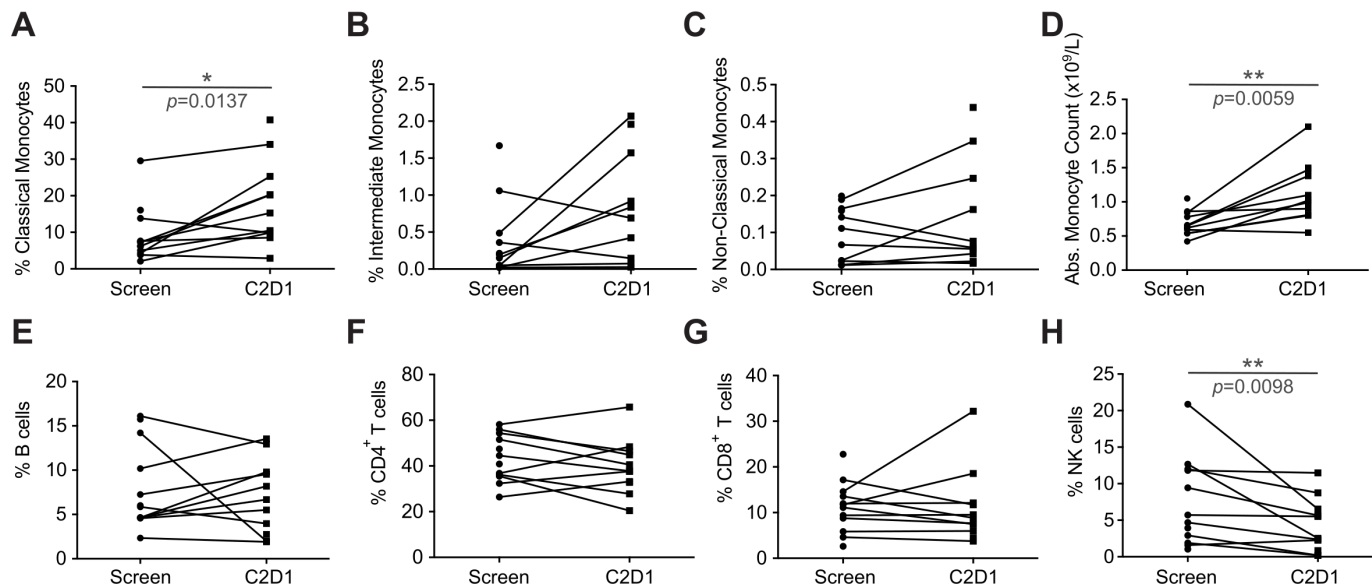Patients received combination therapy of ibrutinib with gemcitabine and nab-paclitaxel in both the dose

Figure 5 Effect of ibrutinib, gemcitabine and nab-paclitaxel combination therapy on immune cells in the blood. Blood samples from patients in both the dose escalation (online supplemental figure 1A) and immune response (online supplemental figure 1B) arms of the study were collected at screen and at the end of one cycle (cycle 2, day 1; C2D1) of ibrutinib plus gemcitabine and nab-paclitaxel combination therapy. Shown are the paired frequencies of (A) classical monocytes, (B) intermediate monocytes, (C) non-classical monocytes, (E) CD19$^+$ B cells, (F) CD4$^+$ T cells, (G) CD8$^+$ T cells, and (H) NK cells, in the blood circulation at screen and at C2D1 of combination therapy as assessed by cytometry by time of flight staining and conventional cell gating on Cytobank. (D) Absolute monocyte counts in blood at screen and at C2D1 of combination therapy that was collected as part of complete blood count counts for blood (all panels: n=12 screen, n=11 C2D1). Wilcoxon matched-pairs signed-rank test was used to test for statistical significance for data in the bar graphs. *p<0.05; **p<0.01; ***p<0.005. NK, natural killer.

escalation and immune response arms starting at cycle 1, day 1 (online supplemental figure 1A,B). Patients from both cohorts were collectively assessed at screen and at the end of the first cycle of combination therapy, that is, at cycle 2, day 1 (C2D1), to study the effects of combination therapy on leukocyte abundance and function in the peripheral blood. Significant increase in classical monocyte frequency was observed at C2D1 (figure 5A). A noticeable trend towards increased frequencies of intermediate (figure 5B) and non-classical monocytes (figure 5C) was also observed. In line with increased percentages, absolute monocyte counts in blood were also increased at C2D1 (figure 5D). A significant reduction in the frequency of natural killer cells was also revealed (figure 5H). However, no significant changes were observed in the frequency of lymphocytes such as B cells (figure 5E), CD4$^+$ T cells (figure 5F), CD8$^+$ T cells (figure 5G) or Tregs (data not shown) with combination therapy. No significant changes in the functional status of immune cells were observed after combination therapy (data not shown).

Effect of ibrutinib therapy on BCR and TCR clonality and association with clinical response

Ibrutinib monotherapy increased BCR clonality in four of six patients (figure 6A) but had no impact as combination therapy (online supplemental figure 7A, left panel). Both ibrutinib monotherapy and combination therapy tended to reduce TCR clonality (figure 6D and online supplemental figure 7A, right panel).

Association of BCR/TCR clonality with clinical response was also assessed collectively in patients from both the study arms before and after the start of combination chemotherapy treatment cycles. Clonality in patients that had either progressive disease or stable disease (PDSD) was compared with those who had partial response (PR) at screen, the end of one (C2D1) or two (C3D1) combination chemotherapy cycles (figure 6B,E). Between the two clinical response groups (PDSD vs PR), BCR clonality was not significantly different before the start of therapy (screen time point) or at the end of one (C2D1) or two (C3D1) combination chemotherapy cycles (figure 6B). In contrast, TCR clonality was lower in the PR patients compared with the PDSD patients at all time points assessed, that is, screen, C2D1 and C3D1 (figure 6E). Hence, lower TCR clonality in PR patients existed prior to therapy and was maintained during at least two cycles of combination chemotherapy, with the difference at the end of the first cycle, that is, at C2D1, reaching statistical significance. When examining the proportion of newly generated clones at C2D1 over screen, PR patients had significantly higher levels of newly generated BCR clones (figure 6C). Similarly, PR patients had greater proportions of newly generated TCR clones at C2D1 over screen, although this difference did not reach statistical significance. Further, median OS trended to be greater in patients that had lower BCR clonality (≤0.01; 9.9 months OS) than in patients with higher BCR clonality (>0.01; 7.74 months OS) (figure 6G). Similarly, median OS trended to be greater in patients with lower TCR clonality (<0.13; 9.9 months OS) than in patients with
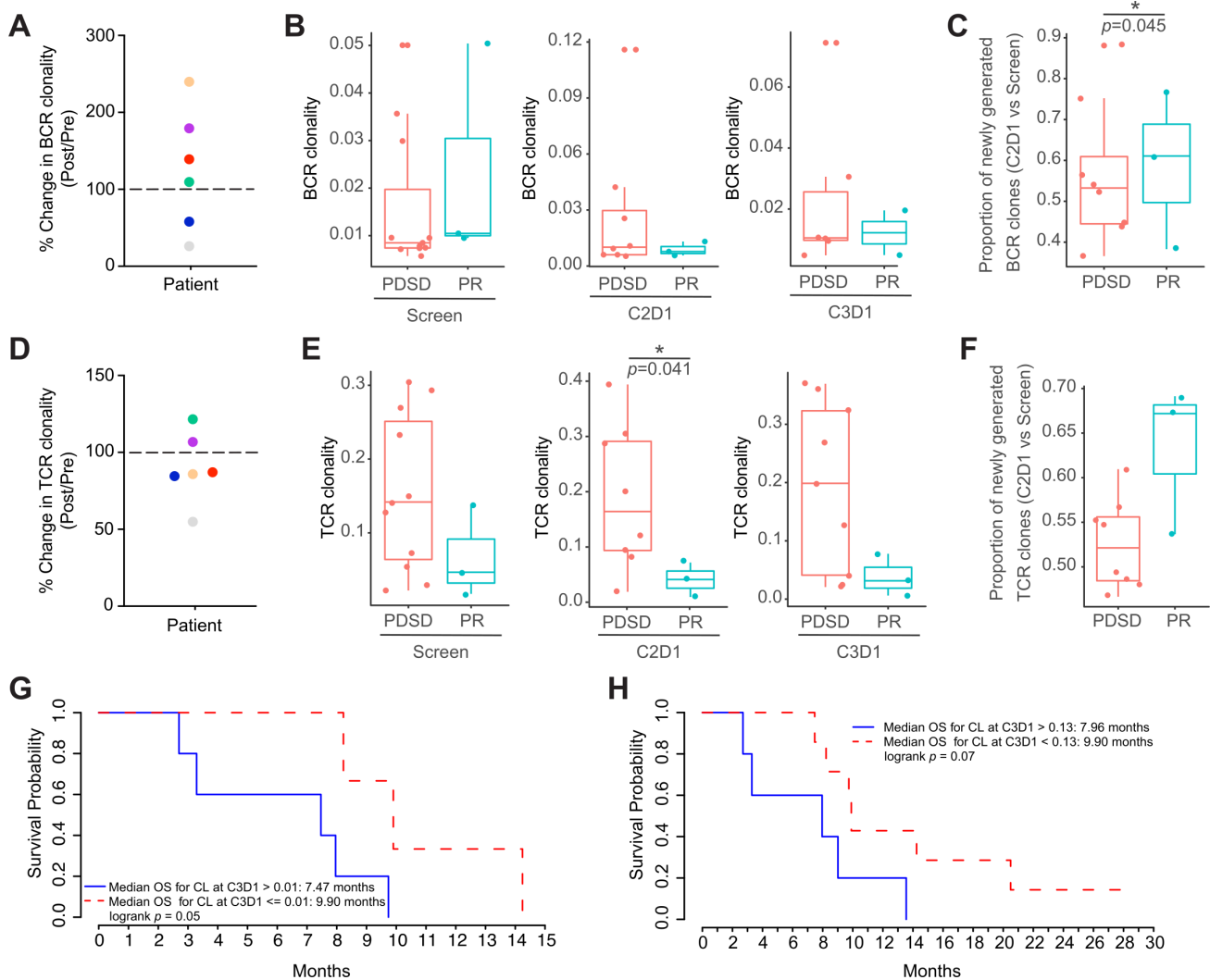
Figure 6 Effect of ibrutinib on B and T-cell receptor clonality and association with clinical response. (A, D) Each colored symbol (pre-ibrutinib=round; post-ibrutinib=square) consistently represents a unique patient in the immune response arm of the study (online supplemental figure 1B). (A) Per cent change (post/pre 1 week ibrutinib treatment) in B-cell receptor (BCR) clonality after 1 week ibrutinib treatment is shown for patients (n=6) in the immune response arm of the study. (B) BCR clonality at (left panel) screen time point, that is, before therapy initiation (n=11 PDSD, n=3 PR), (middle panel) after one cycle of combination therapy (cycle 2, day 1; C2D1) (n=8 PDSD, n=3 PR), and (right panel) after two cycles of combination therapy (cycle 3, day 1; C3D1) (n=6 PDSD, n=2 PR) with ibrutinib, gemcitabine and nab-paclitaxel for patients from both the dose escalation arm and the immune response arm grouped by best clinical response (PDSD, patients with progressive disease or with stable disease; PR, patients with partial response). (C) Proportion of newly generated BCR clones at the end of one cycle of chemotherapy (C2D1/screen) for patients from both the dose escalation and the immune response arms grouped by best clinical response (PDSD, patients with progressive disease or with stable disease; PR, patients with partial response) (n=8 PDSD, n=3 PR). (D) Per cent change (post/pre 1 week ibrutinib treatment) in T-cell receptor (TCR) clonality after 1 week ibrutinib treatment is shown for patients (n=6) in the immune response arm of the study. (E) TCR clonality at (left panel) screen time point, that is, before therapy initiation (n=11 PDSD, n=3 PR), (middle panel) after one cycle of combination therapy (cycle 2, day 1; C2D1) (n=8 PDSD, n=3 PR), and (right panel) after two cycles of combination therapy (cycle 3, day 1; C3D1) (n=9 PDSD, n=3 PR) with ibrutinib, gemcitabine and nab-paclitaxel for patients from both the dose escalation arm and the immune response arm grouped by best clinical response (PDSD, patients with progressive disease or with stable disease; PR, patients with partial response). (F) Proportion of newly generated TCR clones at the end of one cycle of chemotherapy (C2D1/screen) for patients from both the dose escalation and the immune response arms grouped by best clinical response (PDSD, patients with progressive disease or with stable disease; PR, patients with partial response) (n=8 PDSD, n=3 PR). (G) Kaplan-Meier survival curve for patients from both the dose escalation arm and the immune response arm grouped by BCR clonality less than (n=3) or greater than (n=5) 0.01 at the end of two cycles (cycle 3, day 1; C3D1) of combination therapy with ibrutinib, gemcitabine and nab-paclitaxel in both arms. (H) Kaplan-Meier survival curve for patients from both the dose escalation arm and the immune response arm grouped by TCR clonality less than (n=7) or greater than (n=5) 0.13 at the end of two cycles (cycle 3, day 1; C3D1) of combination therapy with ibrutinib, gemcitabine and nab-paclitaxel in both arms. (B, C, E and F) Data plotted in the box plots are median and IQR; Mann-Whitney test was used to test for statistical significance. (G and H) Log-rank test was used to test for statistical significance of the survival curves. *p<0.05; **p<0.01; ***p<0.005.

higher TCR clonality (>0.13; 7.96 months OS) (figure 6H). Taken together, these findings indicated that lower BCR and TCR clonality and greater proportions of newly generated BCR and TCR clones were associated with improved clinical outcomes in this study.

Associations of functional states of blood leukocytes at the end of one cycle of combination chemotherapy (C2D1) with clinical responses for patients in both study arms was also examined. No statistically significant findings emerged due to the small numbers of patients in the study. However, similar trends were observed in functional states of blood leukocytes in the PR patients, as compared with PDSD patients, or in patients that had OS greater than 6 months compared with those with OS less than 6 months (online supplemental figure 7B).

DISCUSSION

This report provides a detailed description of the immunomodulatory effects of ibrutinib monotherapy and combination therapy with the standard regimen of gemcitabine and nab-paclitaxel in patients with advanced PDAC. Although this study is limited in the numbers of patients enrolled, it provides critical clues into the effect of ibrutinib therapy on the immune response, which may inform study design for future clinical trials.

Although ibrutinib is known to reduce B-cell survival and is Food and Drug Administration-approved for chronic lymphocytic leukemia treatment, the effect on B-cell frequency was modest in this study. This might reflect the differential sensitivity of 'normal' non-malignant versus malignant B cells to BTK inhibition. Since ibrutinib is rapidly cleared from the circulation, the mild effect observed on B-cell depletion might also reflect B-cell repopulation between the end of ibrutinib monotherapy and blood and tumor biopsy sampling. Interestingly, consistently increased presence of IL-10^{+} B cells, likely Breg cells, in the TME could be an acquired resistance mechanism. While it is possible that the significant increase in Ki-67^{+} cells in a B-cell cluster in the blood ibrutinib monotherapy represents Bregs, this cannot be conclusively determined as the CyTOF panel did not evaluate IL-10. A recent single cell RNA sequencing study of pancreatic cancer biopsies reported infiltration of both primary and metastatic tumors with B cells with a much greater infiltration in metastatic tumors compared with primary tumors,[22] and thus supporting a negative correlation between disease severity and the extent of B-cell filtration.

In line with previous preclinical findings,[9] ibrutinib monotherapy led to increased frequency of blood monocytes and a trend towards more mature DCs in the TME. This correlated with increased frequency of ICOS^{+} CD4^{+} activated T cells in the periphery and a trend towards fewer dysfunctional CD8^{+} T cells in the TME. Interestingly, the frequency of ICOS^{+} CD4^{+} T cells has been previously reported to increase with anti-cytotoxic T-lymphocytes-associated protein 4 immune checkpoint blockade immunotherapy, where they are critical for antitumor responses.[23 24] Further, these ICOS^{+} CD4^{+} T

cells could potentially represent cells that are destined to become tumor tissue resident memory (TRM) cells.[25] However, this could not be confirmed as none of the staining panels included CD103, a marker of TRM cells. Tertiary lymphoid structures, which are densely packed with leukocytes[26] and associated with improved prognosis and survival in PDAC,[27 28] were not seen in any of the tumor biopsies. The numbers of cells in the available tissue biopsies in addition to the low *n* numbers were insufficient to draw any significant conclusions with spatial analyses. Sufficient tumor biopsy sample was not available to perform RNA-based analyses, such as by the NanoString platform or by single cell RNA sequencing.

Interestingly, the results observed with ibrutinib monotherapy were distinct from those observed when ibrutinib was combined with chemotherapy. Although a significant increase in peripheral blood monocyte frequency was observed both with monotherapy and combination treatment, neither B-cell frequency reduction nor T-cell activation was observed in the blood with combination therapy, raising questions about how the standard chemotherapeutic drugs in PDAC therapy interact with ibrutinib, an immunomodulatory drug. The blunting of ibrutinib-induced immunomodulation when gemcitabine and nab-paclitaxel were concurrently administered may reflect the cytotoxic effects of these chemotherapies on the different immune cells that may have been modulated by the ibrutinib. This might also possibly explain the lack of clinical benefit, as measured by OS and PFS, in the phase III RESOLVE clinical trial for the same combination.[29]

As patients with PDAC with a partial clinical response had trends towards lower T-cell clonality prior to the start of treatment with only minor transient effects from combination therapy, this indicated that these patients likely had pre-existing or natural functional tumor-reactive T cells in their peripheral blood as has been reported previously,[30–32] but the activity of which was not enhanced by ibrutinib, gemcitabine and nab-paclitaxel combination therapy. Sufficient tumor tissue was not available to analyze the BCR and TCR repertoire in the TME.

Similar to findings herein, immune subset analysis of the TME in a phase II trial of acalabrutinib, also a BTK inhibitor, with and without pembrolizumab in patients with advanced head and neck squamous cell carcinoma, showed increased proportion of Tbet^{+} EOMES^{+} late effector CD8^{+} T cells from baseline in four of seven patients receiving combination therapy as compared with pembrolizumab monotherapy, although also without clinical efficacy.[33] Moreover, in a phase II trial of patients with advanced PDAC, acalabrutinib either alone or in combination with pembrolizumab that also failed to show clinical benefit, reported reduced presence of CD15^{+} granulocytic, but not monocytic cells, and evidence of T-cell activation based on increased mean fluorescence intensity of CD69 on both CD4^{+} and CD8^{+} memory (CD45RO^{+}) T cells in the combination arm in the periphery.[34]

In conclusion, the current study revealed that ibrutinib monotherapy induced immunomodulatory

changes in vivo in patients with PDAC, with some stimulatory (T cell, monocyte and DC activation) and inhibitory effects (increased B$_{regs}$). Our results also demonstrate the significant interaction between ibrutinib and chemotherapy. Future studies will need to define whether other therapies could work synergistically with ibrutinib-induced immunomodulation to enhance antitumor responses.

Author affiliations
[1]Division of Hematology/Oncology, Department of Medicine, University of California, San Francisco, California, USA
[2]Department of Cell, Developmental & Cancer Biology, Oregon Health & Science University, Portland, Oregon, USA
[3]Department of Biostatistics, University of California, San Francisco, California, USA
[4]AbbVie, Irvine, California, USA
[5]Department of Medicine, Oregon Health & Science University, Portland, Oregon, USA
[6]Medical Oncology, Providence Portland Medical Center, Portland, Oregon, USA
[7]Parker Institute for Cancer Immunotherapy, San Francisco, California, USA

Data availability statement Data are available upon reasonable request. All data relevant to the study are included in the article or uploaded as supplementary information. Mass cytometry data will be shared publicly on Flow Repository while R-based analysis codes will be made publicly available on GitHub upon request. No novel materials were generated as part of this study.

ORCID iDs
Meenal Sinha http://orcid.org/0000-0002-4008-4080
Eric Liu http://orcid.org/0000-0003-2286-0856
Alexander Cheung http://orcid.org/0000-0002-2115-6966

REFERENCES

1 Von Hoff DD, Ervin T, Arena FP, *et al*. Increased survival in pancreatic cancer with nab-paclitaxel plus gemcitabine. *N Engl J Med* 2013;369:1691–703.
2 Poch B, Lotspeich E, Ramadani M, *et al*. Systemic immune dysfunction in pancreatic cancer patients. *Langenbecks Arch Surg* 2007;392:353–8.
3 Jaffee EM, Hruban RH, Biedrzycki B, *et al*. Novel allogeneic granulocyte-macrophage colony-stimulating factor-secreting tumor vaccine for pancreatic cancer: a phase I trial of safety and immune activation. *J Clin Oncol* 2001;19:145–56.
4 Hinz S, Pagerols-Raluy L, Oberg H-H, *et al*. Foxp3 expression in pancreatic carcinoma cells as a novel mechanism of immune evasion in cancer. *Cancer Res* 2007;67:8344–50.
5 Ino Y, Yamazaki-Itoh R, Shimada K, *et al*. Immune cell infiltration as an indicator of the immune microenvironment of pancreatic cancer. *Br J Cancer* 2013;108:914–23.
6 Hiraoka N, Onozato K, Kosuge T, *et al*. Prevalence of FOXP3+ regulatory T cells increases during the progression of pancreatic ductal adenocarcinoma and its premalignant lesions. *Clin Cancer Res* 2006;12:5423–34.
7 Shibuya KC, Goel VK, Xiong W, *et al*. Pancreatic ductal adenocarcinoma contains an effector and regulatory immune cell infiltrate that is altered by multimodal neoadjuvant treatment. *PLoS One* 2014;9:e96565.
8 Blando J, Sharma A, Higa MG, *et al*. Comparison of immune infiltrates in melanoma and pancreatic cancer highlights VISTA as a potential target in pancreatic cancer. *Proc Natl Acad Sci U S A* 2019;116:1692–7.
9 Gunderson AJ, Kaneda MM, Tsujikawa T, *et al*. Bruton tyrosine kinase-dependent immune cell cross-talk drives pancreas cancer. *Cancer Discov* 2016;6:270–85.
10 Massó-Vallés D, Jauset T, Serrano E, *et al*. Ibrutinib exerts potent antifibrotic and antitumor activities in mouse models of pancreatic adenocarcinoma. *Cancer Res* 2015;75:1675–81.
11 Sinha M, Griffith M, Betts C, Choe G, *et al*. Immune modulatory effects of ibrutinib in pancreatic ductal adenocarcinoma. *Annals of Oncology* 2019;30:iv40.
12 Spitzer MH, Nolan GP. Mass cytometry: single cells, many features. *Cell* 2016;165:780–91.
13 Spitzer MH, Carmi Y, Reticker-Flynn NE, *et al*. Systemic immunity is required for effective cancer immunotherapy. *Cell* 2017;168:487–502.
14 Tsujikawa T, Kumar S, Borkar RN, *et al*. Quantitative multiplex immunohistochemistry reveals Myeloid-Inflamed Tumor-Immune complexity associated with poor prognosis. *Cell Rep* 2017;19:203–17.
15 Banik G, Betts CB, Liudahl SM, *et al*. High-dimensional multiplexed immunohistochemical characterization of immune contexture in human cancers. *Methods Enzymol* 2020;635:1–20.

16 Liudahl SM, Betts CB, Sivagnanam S, *et al*. Leukocyte heterogeneity in pancreatic ductal adenocarcinoma: phenotypic and spatial features associated with clinical outcome. *Cancer Discov* 2021;11:2014–31.

17 Schindelin J, Arganda-Carreras I, Frise E, *et al*. Fiji: an open-source platform for biological-image analysis. *Nat Methods* 2012;9:676–82.

18 Carpenter AE, Jones TR, Lamprecht MR, *et al*. CellProfiler: image analysis software for identifying and quantifying cell phenotypes. *Genome Biol* 2006;7:R100.

19 Zhang L, Cham J, Paciorek A, *et al*. 3D: diversity, dynamics, differential testing - a proposed pipeline for analysis of next-generation sequencing T cell repertoire data. *BMC Bioinformatics* 2017;18:129.

20 Zhang L, Kandadi H, Yang H, *et al*. Long-term sculpting of the B-cell repertoire following cancer immunotherapy in patients treated with Sipuleucel-T. *Cancer Immunol Res* 2020;8:1496–507.

21 Chen LS, Bose P, Cruz ND, *et al*. A pilot study of lower doses of ibrutinib in patients with chronic lymphocytic leukemia. *Blood* 2018;132:2249–59.

22 Lee JJ, Bernard V, Semaan A, *et al*. Elucidation of tumor-stromal heterogeneity and the ligand-receptor interactome by single-cell transcriptomics in real-world pancreatic cancer biopsies. *Clin Cancer Res* 2021;27:5912–21.

23 Fu T, He Q, Sharma P. The ICOS/ICOSL pathway is required for optimal antitumor responses mediated by anti-CTLA-4 therapy. *Cancer Res* 2011;71:5445–54.

24 Ng Tang D, Shen Y, Sun J, *et al*. Increased frequency of ICOS+ CD4 T cells as a pharmacodynamic biomarker for anti-CTLA-4 therapy. *Cancer Immunol Res* 2013;1:229–34.

25 Peng C, Huggins MA, Wanhainen KM, *et al*. Engagement of the costimulatory molecule ICOS in tissues promotes establishment of CD8$^+$ tissue-resident memory T cells. *Immunity* 2022;55:98–114.

26 Sautès-Fridman C, Petitprez F, Calderaro J, *et al*. Tertiary lymphoid structures in the era of cancer immunotherapy. *Nat Rev Cancer* 2019;19:307–25.

27 J Gunderson A, Rajamanickam V, Bui C, *et al*. Germinal center reactions in tertiary lymphoid structures associate with neoantigen burden, humoral immunity and long-term survivorship in pancreatic cancer. *Oncoimmunology* 2021;10:1900635.

28 Hiraoka N, Ino Y, Yamazaki-Itoh R, *et al*. Intratumoral tertiary lymphoid organ is a favourable prognosticator in patients with pancreatic cancer. *Br J Cancer* 2015;112:1782–90.

29 Tempero M, Oh D-Y, Tabernero J, *et al*. Ibrutinib in combination with nab-paclitaxel and gemcitabine for first-line treatment of patients with metastatic pancreatic adenocarcinoma: phase III resolve study. *Ann Oncol* 2021;32:600–8.

30 Schmitz-Winnenthal FH, Escobedo LVG, Beckhove P, *et al*. Specific immune recognition of pancreatic carcinoma by patient-derived CD4 and CD8 T cells and its improvement by interferon-gamma. *Int J Oncol* 2006;28:1419–28.

31 Schmitz-Winnenthal FH, Volk C, Z'graggen K, *et al*. High frequencies of functional tumor-reactive T cells in bone marrow and blood of pancreatic cancer patients. *Cancer Res* 2005;65:10079–87.

32 Kubuschok B, Neumann F, Breit R, *et al*. Naturally occurring T-cell response against mutated p21 ras oncoprotein in pancreatic cancer. *Clin Cancer Res* 2006;12:1365–72.

33 Taylor MH, Betts CB, Maloney L, *et al*. Safety and efficacy of pembrolizumab in combination with Acalabrutinib in advanced head and neck squamous cell carcinoma: phase 2 proof-of-concept study. *Clin Cancer Res* 2022;28:903–14.

34 Overman M, Javle M, Davis RE, *et al*. Randomized phase II study of the Bruton tyrosine kinase inhibitor acalabrutinib, alone or with pembrolizumab in patients with advanced pancreatic cancer. *J Immunother Cancer* 2020;8:e000587.